MASTER

MONITORING THE VADOSE ZONE IN FRACTURED TUFF, YUCCA MOUNTAIN, NEVADA

Parviz Montazer[1], E. P. Weeks[1], Falah Thamir[2], S. N. Yard[2], and P. B. Hofrichter[3]

[1]U.S. Geological Survey, Denver, Colorado

[2]Goodson & Associates, Denver, Colorado

[3]Holmes & Narver, Inc., Las Vegas, Nevada

CONF-8511172--8

DE86 008850

Abstract

Unsaturated tuff beneath Yucca Mountain, Nevada, is being evaluated by the U.S. Department of Energy as a host rock for a potential repository for high-level radioactive waste. As part of the Nevada Nuclear Waste Storage Investigations Project of the U.S. Department of Energy, the U.S. Geological Survey has been conducting hydrologic, geologic, and geophysical investigations at Yucca Mountain and the surrounding region to provide data for evaluation of the potential suitability of the site. Hydrologic investigations of the unsaturated zone at this site were started in 1982. A 17.5-inch- (44.5-centimeter-) diameter borehole (USW UZ-1) was drilled by the reverse-air vacuum-drilling technique to a depth of 1,269 feet (387 meters). This borehole was instrumented at 33 depth levels. At 15 of the levels, 3 well screens were embedded in coarse-sand columns. The sand columns were isolated from each other by thin layers of bentonite, columns of silica flour, and isolation plugs consisting of expansive cement. Thermocouple psychrometers and pressure transducers were installed within the screens and connected to the data-acquisition system at the land surface through thermocouple and logging cables. Two of the screens at each level were equipped with access tubes to allow collection of pore-gas samples. In addition to these instruments, 18 heat-dissipation probes were installed within the columns of silica flour, some of which also had thermocouple psychrometers.

After more than 2 years of monitoring, the majority of the instruments were still functioning and producing reasonable data. A slow recovery from the disturbed state to natural conditions was detected during the first 90 days of monitoring; this recovery probably was the result of the large diameter of the borehole. Preliminary results indicated that suction pressures for the welded units ranged from -2 to -15 bars (-0.2 to -1.5 megapascals). Reasonable agreement existed between data from psychrometers

and from heat-dissipation probes, except where silica flour was not in equilibrium with the formation. Water fluxes estimated in the repository host-rock unit range from 4×10^{-3} to 2×10^{-2} inch per year (0.1 to 0.5 millimeter per year) using matric-potential distribution, and from -1×10^{-3} to -2×10^{-3} inch per year (-0.025 to -0.05 millimeter per year) using geothermal gradient.

Responses to short-term barometric fluctuations were detected to a maximum depth of about 300 feet (91 meters) in the borehole. Below this depth, only long-term barometric fluctuations were detectable. Equivalent effective hydraulic conductivity, estimated from air permeability, ranged from 0.6 to 2 feet per day (0.2 to 0.6 meters per day).

Introduction

Mechanisms of fluid flow through thick unsaturated zones consisting of heterogeneous fractured rocks, are not well understood. The extensively fractured welded tuff and the less-fractured nonwelded and bedded tuff at Yucca Mountain, Nevada, result in a complex flow system, that cannot be characterized readily by the conventional techniques used to monitor shallow unsaturated soils. Some complexities of fluid flow through unsaturated fractured tuff at Yucca Mountain are discussed by Montazer and Wilson (1984).

Instrumentation and monitoring of unsaturated fractured tuff in deep boreholes have not been attempted previously. The purpose of this study is to evaluate the results obtained from instrumenting a deep test borehole (borehole USW UZ-1; Whitfield, 1985, this proceedings), in unsaturated tuff, and to understand the mechanisms of fluid flow in such hydrologic systems.

Instrumentation and testing of the unsaturated fractured tuff have been hampered by the difficulties inherent in installation of instruments and interpretation of the results. Evans (1983) reviewed the state of the art of instrumentation technology applicable to monitoring these types of rocks. Montazer (1982) discussed the problems associated with testing unsaturated fractured metamorphic rocks. Although, in the past few years, many investigators have begun research on characterization of unsaturated fractured tuff, the authors are unaware of other attempts to install instruments in unsaturated fractured rocks in deep boreholes.

Characterization of the fluid flow in any hydrologic system requires measurements of the fluid-transport properties of the medium and the distribution of potential energy within the fluids. Chemical composition of dissolved substances in the liquid phase and gas phase can aid in understanding the mechanisms and history of fluid transport within the hydrologic system.

This paper describes the methods used to install instruments in a test borehole drilled to a depth of 1,269 ft (387 m), and also presents some preliminary results from monitoring these instruments. Some problems with interpretation of the results also are discussed. Hydrologic

characteristics of the site are described by Montazer and Wilson (1985, this proceedings). Drilling methods and specific information about the borehole are described by Whitfield (1985, this proceedings).

This investigation is one of many by the U.S. Geological Survey that are underway at Yucca Mountain, as part of the Nevada Nuclear Waste Storage Investigations Project of the Department of Energy, Nevada Operations Office, under Interagency Agreement DE-AI08-78ET44802.

Measurement of Fluid Potential

Knowledge of the distribution of fluid potential energy (or potential) is needed to understand fluid flow in the unsaturated zone. Fluid potentials that are important in unsaturated-zone flow are: (1) Matric, or pressure, potential in the liquid phase; (2) liquid-phase gravitational potential; (3) gas-phase pressure (or pneumatic) and gravitational potentials; (4) osmotic potential; and (5) thermal potential, or downhole temperature for a given fluid phase. Combined pressure and gravitational potential represent total potential; fluid movement occurs down the total potential gradient. Concepts of these potentials and methods for their measurements are described by Evans (1983), Morrison (1983), Stallman (1964), and Remson and Randolph (1962).

Pneumatic-pressure potentials were measured by downhole, semiconductor, pressure transducers. Downhole rather than surface measurements were made to avoid time lag and pressure loss through the 1/8-in.-(3.2-mm-) diameter tubing, particularly during planned air withdrawal or injection tests. The transducers were aged before installation to minimize their inherent, exponentially decreasing drift.

Matric potentials were measured using heat-dissipation probes (HDP); combined matric and osmotic potentials (termed water potentials) were measured by thermocouple psychrometers (TP), as described by Thamir and McBride (1985, this proceedings). Tensiometers were not installed because of difficulties of installation in deep boreholes and because of their limited range of sensitivity. Heat-dissipation probes can be calibrated for matric potentials that range from -0.1 to -5 bars (-0.01 to -0.5 megapascals; however, an attempt was made to calibrate the probes to -15 bars (-1.5 megapascals) for this study. Thermocouple psychrometers were calibrated and used for measuring water potentials from -5 to -75 bars (-0.5 to -7.5 megapascals). A major limitation of the TP data is that the matric potential generally is the variable of interest, rather than the combined matric and osmotic-pressure potential, or water potential. For this study, osmotic potentials were determined to be insignificant; therefore, they are ignored hereafter, and the TP measurements are called matric potentials. Temperature measurements also were made from the output of copper-constantan thermocouple junctions that are part of the TP.

Emplacement of the Instruments

After drilling and logging test borehole USW UZ-1 (Whitfield, 1985; and Palaz, 1985, this proceedings), 15 depth zones were selected for installation of pressure transducers, TP, and access tubes. These depth locations were designated by instrument stations (IS) 1 through 15. At each IS, sensors were housed in one of three well screens (fig. 1), and designated A, B, and C from top to bottom. The top well screen (A) contained a TP and was connected to the land surface by an access tube for gas sampling. The middle well screen (B) housed a TP and a pressure transducer. The bottom well screen (C) contained a pressure transducer and was connected to an access tube for gas sampling, and for checking calibration and proper functioning of the pressure transducer.

In addition to these IS, 18 different depths were selected for installation of HDP, 5 of which were accompanied by TP. These HDP were designated as HDP-A or HDP-B depending on whether they were located above (HDP-A) or below (HDP-B) the nearby IS. The TP associated with these HDP were designated as HDP-TP.

Assembly and Installation of the Instruments

Prior to installation, the sensors were calibrated with cable lengths cut for the predesignated depths of installation in the borehole. After calibration, all cables with attached sensors were laid out, and instruments were inserted into the well screens and secured. The HDP were protected with cups filled with saturated silica flour, but they were not housed in well screens. The well screens and the HDP were adjusted, so that they would be located in predesignated-depth intervals. The entire assembly was transported to the test borehole site as a bundle.

To emplace the filler material in the borehole, two tremie pipes were lowered into the borehole prior to installation of the bundle. After tremie-pipe installation, a television camera was lowered in to the borehole to inspect it for obstructions. The bundle then was lowered into the borehole with a 2.38-in. (6.0-cm) outside-diameter fiberglass access tube for geophysical logging. The wires and tubing were encased in polyurethane-foam isolation plugs to prevent gas flow between stations along the wires. The isolation plugs were situated so that they would be surrounded by grout during stemming. Standoffs also were installed on the fiberglass tube near each IS to prevent damage to the instruments by collision with the borehole wall during installation.

Stemming Procedures

When the assembly was lowered into the borehole, dry materials (silica flour, sand, and bentonite) were poured through one tremie pipe, and wet materials (cement and water) were poured through the other tremie pipe to stem the hole. Final configuration of the stemmed borehole and the location of the IS and HDP are shown in figure 2. Actual location of the sensors and the contacts between different materials were determined by geophysical logs run inside the fiberglass tube.

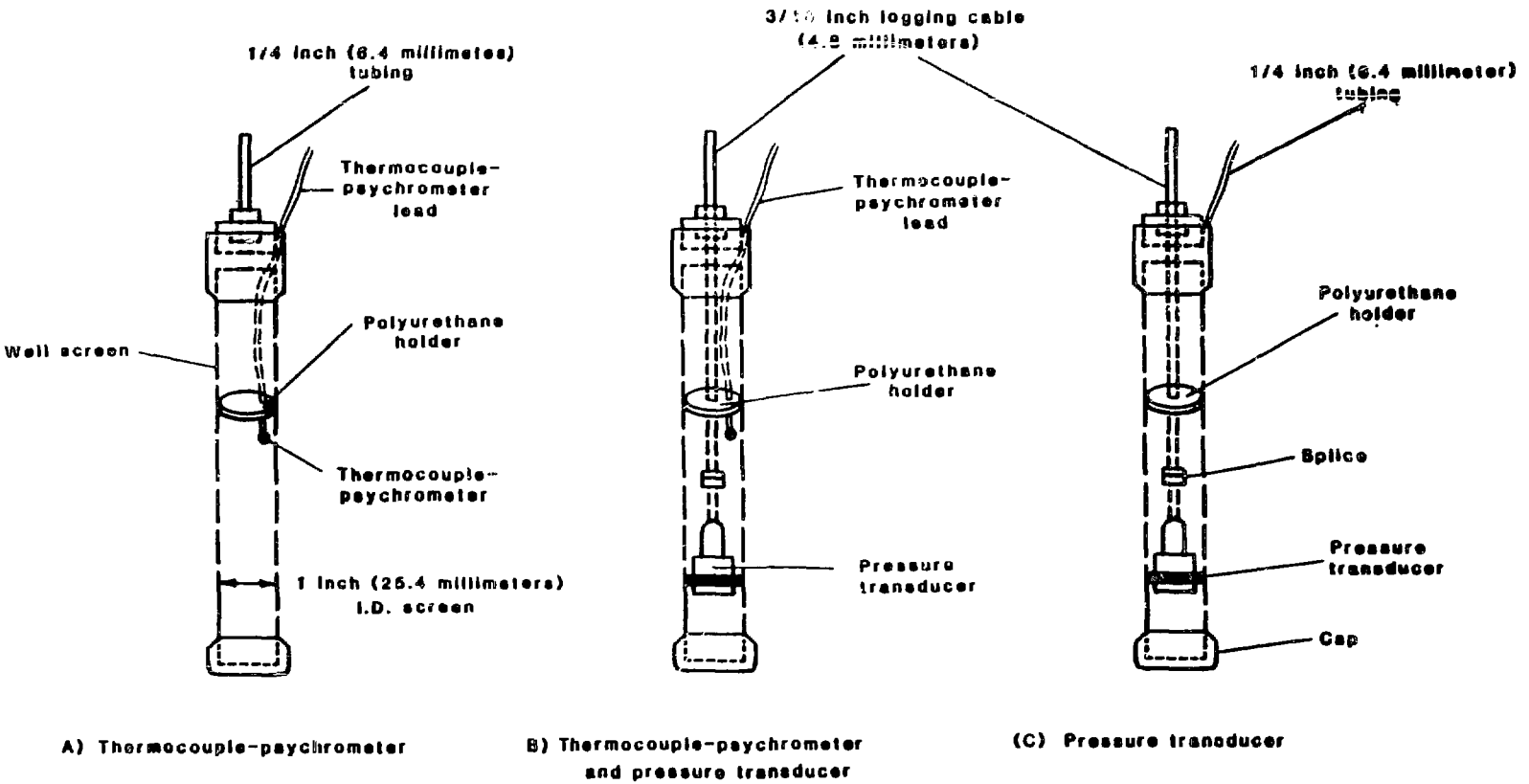

Figure 1.--Schematic diagrams of the well screens, and the types of instruments installed in screens A, B, and C.

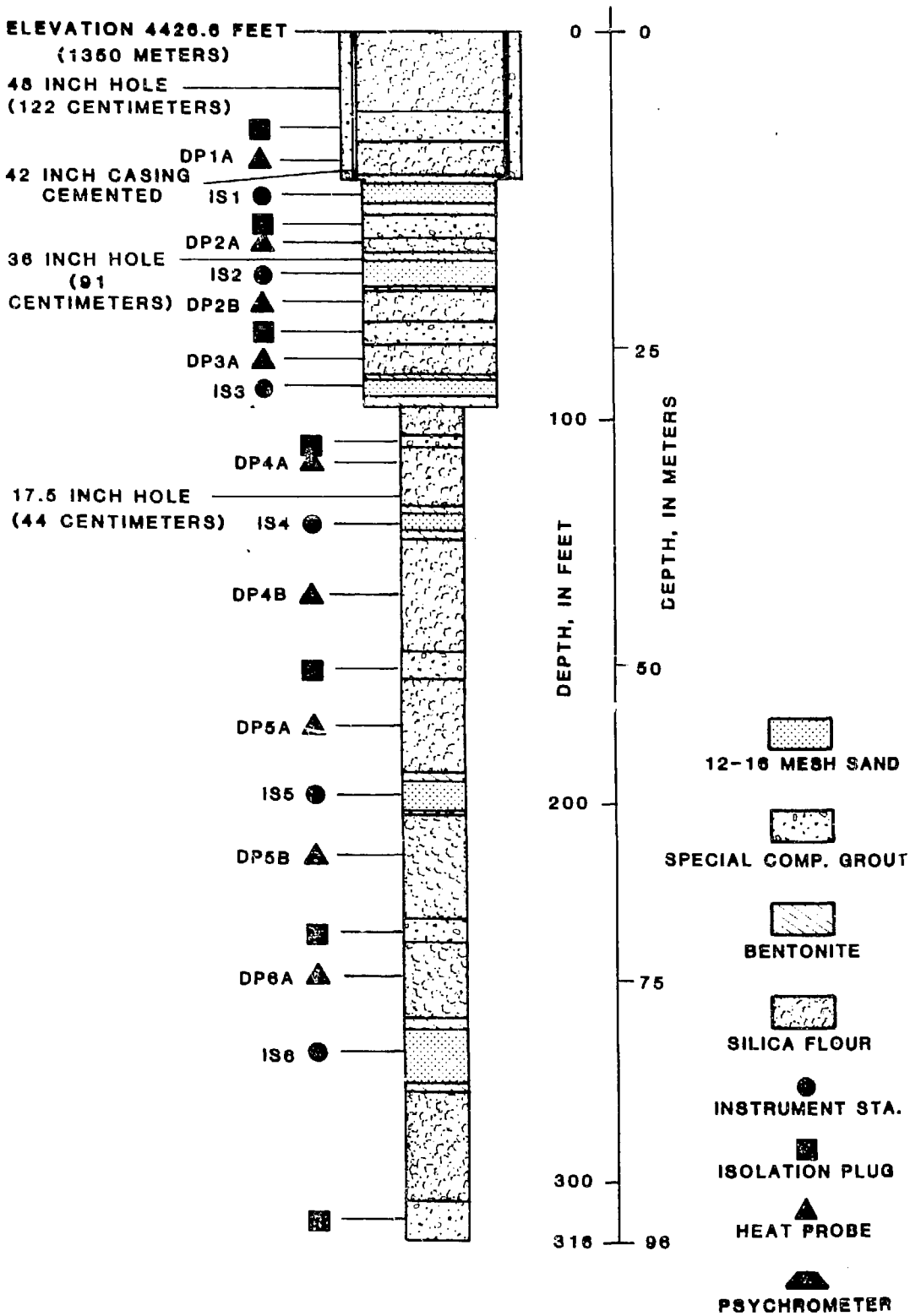

Figure 2.--Details of the stemming of test borehole USW UZ-1.

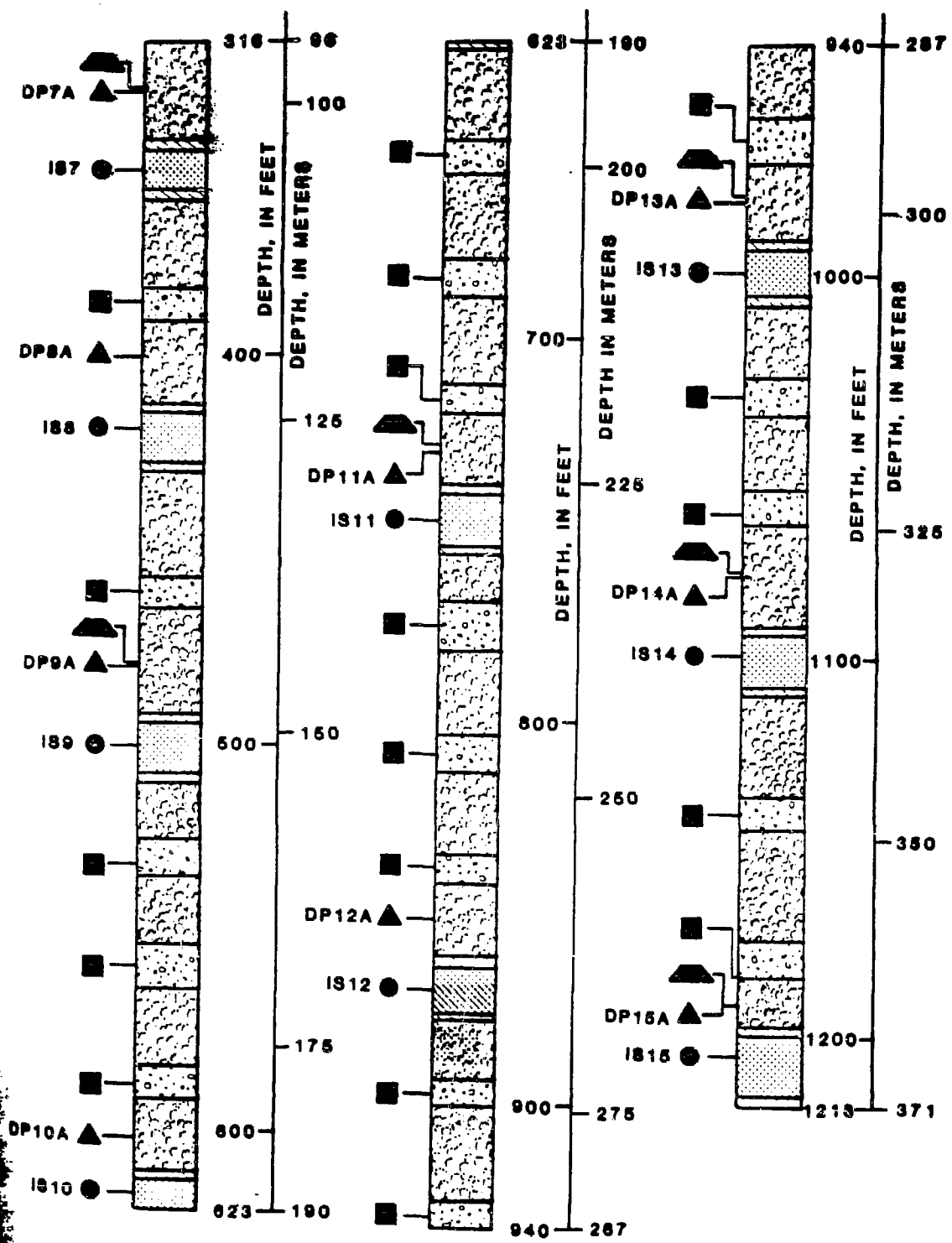

Figure 2.--Details of the stemming of test borehole USW UZ-1--Continued.

Silica flour was selected as the filler material, instead of the crushed tuff that was produced during drilling, because of its uniformity, and, therefore, predictability. The HDP were embedded in the silica flour. The silica flour used to stem the HDP was wetted, prior to installation to a matric potential slightly greater than that predicted for the formation. This procedure was done to prevent the HDP from drying to less than ambient-moisture content before rewetting. Such drying and rewetting would result in hysteresis and would produce data that would not fit the drainage-calibration curve.

Where the silica flour was in contact with the matrix of densely welded tuff, a capillary barrier probably existed that retarded the flow of water from the formation into the silica flour. This retardation could result in additional delays in equilibration time. However, this condition did not exist where silica flour was in contact with fractures or with nonwelded units.

The silica flour was separated from the sand layers by a thin layer of bentonite to decrease further the possibility of gas flow from one zone to the other. The bentonite needed to become nearly saturated to establish equilibrium with the formation, thereby attaining minimum permeability to air.

The grout limited the movement of the gases between adjacent IS within the borehole. In addition, the grout layer supported the column of the silica flour, minimizing settlement of the flour, that could create large air cavities.

The well screens housing TP and transducers were embedded in coarse dry sand, because the sensors monitored the formation through the air phase. At the ambient matric potential of the formation, the sand attains very small saturation, and thereby retains large permeability to air.

Data Acquisition

The data-acquisition system is described in detail by Thamir and McBride (1985, this proceedings). During the entire installation operation, the instruments were monitored for proper functioning. After stemming, continuous monitoring was started. During the first 90 d, TP and pressure transducers were scanned every hour, and HDP were scanned twice daily. After this period, TP were scanned twice daily and HDP were scanned once daily. Pressure transducers and thermocouples were sampled twice hourly for the first 90 d; thereafter, they were sampled at least every 2 hours. The data logger was programmed to log more frequently, when significant pressure changes were occurring. The data logger used to measure temperature had much greater input impedence than the data logger used to obtain psychrometric measurements from the TP. The greater input impedence was required to minimize the effect of the length of the lead wires.

A weather station was installed near the test-borehole site to monitor barometric pressure, air temperature, relative humidity, wind speed, and precipitation. These data were logged hourly.

Monitoring Fluid Potentials

Matric Potential

Examples of variations with time of the matric potential measured with HDP are shown in figure 3. Most of the HDP initially measured large matric potentials, because the silica flour was wetter around these probes than elsewhere in the silica-flour column. The matric-potential measurements rapidly decreased as this water dissipated into the silica flour and possibly into the formation. The data for HDP-3A have a different trend. However, the calibration curve for the indicated range for the HDP was based on linear extrapolation from the -5-bar (-0.5 megapascal) range, and the absolute values may not be reliable for matrix potentials less than -5 bars (-0.5 megapascal). Examples of variation of the water potential with time measured by the TP are shown in figure 4. In this case, the water potentials initially were small; they rapidly increased during the first 90 d; and then they increased more slowly. The TP were stemmed within initially dry screened sand. The unsaturated hydraulic conductivity of this sand was extremely small at the presumed ambient-moisture tension in the surrounding medium. Consequently, vapor diffusion into the sand and subsequent sorption on the sand grains probably was the dominant transport process, by which the moisture content of the sand backfill equilibrated with that in the formation. The rate at which this process progressed decreased exponentially with time. Three downward spikes in water potential occurred on November 8, 1985 (fig. 4). These increases in the water potentials occurred during pumping for gas samples; they resulted from the flow of nearly vapor-saturated air through the sand column. This vapor-saturated air increased the humidity around the TP. Soon after pumping stopped, however, the normal trend resumed as vapor condensed on the drier sand without materially changing its matric potential. This phenomenon indicated that, under transient conditions, advection of nearly-saturated air could occur through a relatively dry medium without equilibrating with that medium. IS-1A initially measured large water potentials from October to December 1983 (fig. 4). In December 1983, this TP began measuring very low water potentials. This sudden reversal probably is the result of single-point measurement technique as discussed by Thamir and McBride (1985, this proceedings).

Temperature

Temperature records at various IS, from November 1983 to April 1984, indicated that temperatures of the IS nearly had equilibrated with temperatures in the adjacent formation by mid-November. However, the temperatures at IS-1, IS-2, IS-3, and IS-4 had some variations with time. No seasonal changes would be anticipated at the depths of IS-3 and IS-4; the cause of variation was unknown. In addition, the temperature data for IS-1, IS-4, IS-7, and IS-8 indicate departures from the normal trend; the cause of these variations is not known at this time. Temperature records are available only for IS-3, IS-4, IS-13, IS-14, and IS-15, after April 1984; temperature records for other IS are not available because of data-acquisition problems.

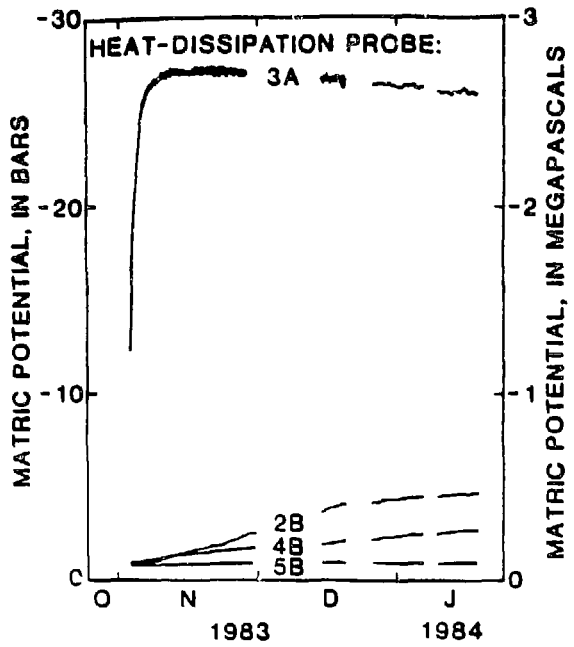

Figure 3.--Variations of matric potential with time, as measured with heat-dissipation probes.

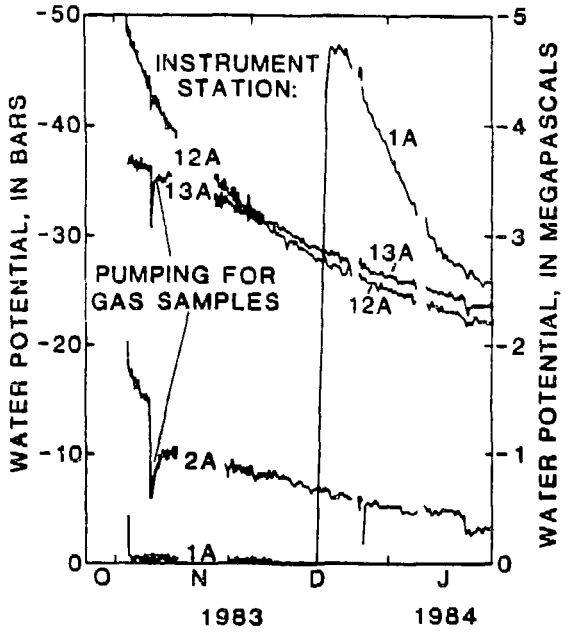

Figure 4.--Variations of water potential with time, as measured wit thermocouple psychrometers installed in instrument stations.

Pneumatic Potential

Data from the downhole-pressure transducers are shown in figure 5 for February 25-27, 1984. Diurnal-pressure changes occurred at most of the IS shown in this figure, in response to more pronounced barometric changes at land surface. At greater depths, pressure responses to diurnal barometric fluctuations were damped out; however, seasonal changes (not shown) occurred. The zero offset was shifted from that obtained during calibration, so that the positions of various curves were not offset necessarily by an amount equal to the gravitational potential in the gas phase. However, these data can be adjusted to provide total pneumatic potential, by subtracting the long-term mean pressure from each transducer record and adding the mean barometric pressure.

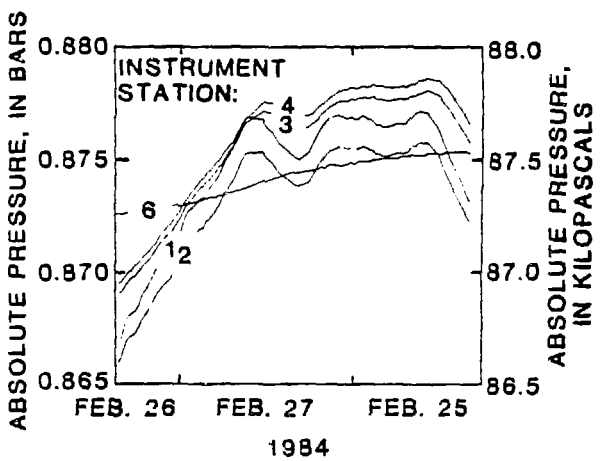

Figure 5.--Downhole-pressure variations at test borehole USW UZ-1, measured with downhole-pressure transducers.

Fluctuations in total pneumatic potential were monitored during the same period, using a differential-pressure transducer connected through a solenoid-valve manifold system to various access tubes at land surface. Data were obtained by opening the valves sequentially using a data-logger actuated multiplexor system; absolute pressure at land surface was monitored using a digital barometer. Results of these measurements are shown in figure 6; these results, in terms of pressure fluctuations, agree well with results obtained using the downhole pressure transducers.

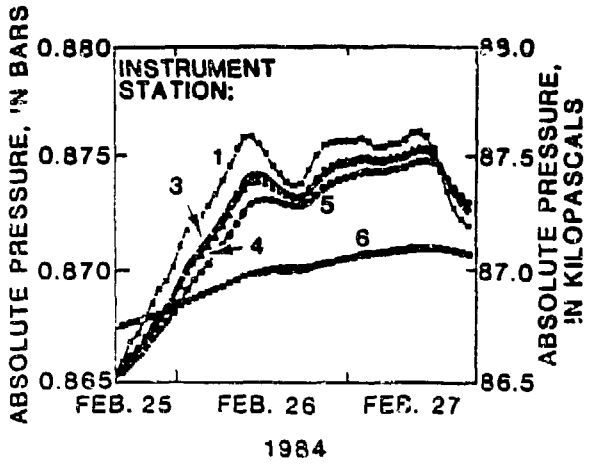

Figure 6.--Adjusted downhole-pressure variations at test borehole USW UZ-1. Differential pressures, measured with uphole transducers, were added to the calculated pneumatic-gravitational potential.

Pneumatic-Gravitational Potential

The change in pneumatic-gravitational potential across each screened interval can be used to determine the actual offset error in the downhole pressure transducers. Moreover, computations of soil-gas density, made as part of the gravitational-potential calculations, can indicate zones in which buoyant gas flow could occur. The changes in pneumatic-gravitational potential across each screen and the pressure potential at each screen are shown in table 1, with the mean January 1984 temperature at each IS and the mean soil-gas density for each screened interval. For the computations, the soil gas was assumed to be saturated with water vapor. The mole density for each screened interval was computed by estimating the midpoint pressure, computing the midpoint temperature, and inserting these values into the ideal gas law. The saturated water-vapor density for the midpoint temperature was obtained from a table (Campbell, 1977), and the moles of water vapor were subtracted from the total number of moles. This remainder was multiplied by the molecular weight of air and added to the water-vapor density to yield total soil-gas density. The change in pneumatic-gravitational potential across each depth interval was computed by the equation:

$$\Delta P_a g = \rho_a g \Delta z;$$

where $\Delta P_a g$ = gravitational potential in the gas phase;
ρ_a = gas density;
g = acceleration due to gravity; and
Δz = depth interval.

In table 1, the soil-gas density in the interval between IS-6 and IS-8 is slightly less dense than in the overlying interval, and air might flow upward by free convection.

Gas samples were collected at various times during the monitoring period. Results of gas sampling are discussed by Yang et al. (1985, this proceedings).

Discussion of the Results

Matric Potential and Flux

Interpretation of the data from TP and HDP in test borehole USW UZ-1 is complicated by the effect of the large volume of backfill material, in which matric potential must equilibrate with the conditions in the formation before accurate measurements can be obtained. As noted before, the TP were installed in initially dry sand, and the HDP were emplaced in locally wetted silica flour. Therefore, the expected trend for the water potential measured by the TP would be from low to high (dry to wet), and the expected trend for the matric potential measured by the HDP would be from high to low (wet to dry). The wet zone created around the HDP in the silica flour was expected to become drier as the water dissipated. The drier sections of the column were expected to absorb water from the formation, and, therefore, to attain equilibrium with the rest of the column.

Variations in average matric potential, as measured by HDP for the months indicated, are shown in figure 7. Seven of the HDP eventually became inoperative, so only a few data are shown for these probes. Heat-dissipation probes 2A, 4A, 5A, and 5B, which were adjacent to alluvium or nonwelded tuff, dried only a little and then essentially remained constant. Heat-dissipation probe 3A showed a reverse response, becoming wetter throughout monitoring. Heat-dissipation probes 8A, 9A, and 15A became progressively drier; but then became wetter in 1985. Heat-dissipation probe 11A had two reversals. Heat-dissipation probe 13A became drier, and then seemed to stabilize.

These results indicate that HDP adjacent to alluvium or nonwelded tuff generally showed a brief drying trend before reaching some equilibrium; whereas HDP adjacent to welded tuff sustained a long-term drying trend with a subsequent wetting trend. The alluvium and nonwelded tuff contained higher moisture contents than did the welded units; therefore, more water was available to wet the silica-flour columns that were adjacent to alluvium and nonwelded tuff than was available to wet the columns adjacent to nonwelded units. In addition, the alluvium and nonwelded tuff had greater matrix hydraulic conductivity than did welded tuff. Also, the silica-flour columns in these alluvium and nonwelded-tuff intervals were

Table 1.--Average January 1984 downhole temperatures, mean density of air between adjacent screens, computed increase in pressure with depth between each screen (ΔP), and computed absolute pressure at each screen, based on the cumulative increase in weight of the air column above the screen. [Air throughout the column is assumed to be saturated with water vapor. Densities were computed for the midpoint temperature and pressure between each screen, except that the temperature from land surface to screen 1 was assumed equal to the temperature at screen 1.]

Screen	Depth interval below land surface		Temperature		Air density		ΔP		Pressure	
	(ft)	(m)	(°F)	(°C)	(lb/ft^3)	kg/m^3	(millibars)	(kPa)	(bar)	(kPa)
LS			--	--					0.869	86.90
	42.1	12.83	--	--	6.39×10^{-2}	1.0234	1.29	0.129		
1			67.75	19.861					0.8703	87.029
	51.0	15.55			6.4×10^{-2}	1.0255	1.56	0.156		
3			67.40	19.666					0.87185	87.185
	37.9	11.55			6.414×10^{-2}	1.0275	1.16	0.116		
4			67.45	19.692					0.87301	87.301
	70.0	21.34			6.421×10^{-2}	1.0286	2.15	0.215		
5			68.15	20.085					0.87516	87.516
	64.8	19.75			6.421×10^{-2}	1.0285	1.99	0.199		
6			69.70	20.947					0.87715	87.715
	82.6	25.17			6.416×10^{-2}	1.0278	2.54	0.254		
7			70.98	21.657					0.87969	87.969
	72.5	22.10			6.415×10^{-2}	1.0276	2.23	0.223		
8			72.31	22.393					0.88192	88.192
	80.6	24.57			6.419×10^{-2}	1.0282	2.48	0.248		
9			72.89	22.716					0.88439	88.439
	119.3	36.36			6.428×10^{-2}	1.0296	3.67	0.367		
10			74.18	23.435					0.88806	88.806
	126.4	38.53			6.430×10^{-2}	1.0310	3.89	0.389		
11			75.48	24.154					0.89195	89.195
	123.9	37.75			6.446×10^{-2}	1.0325	3.82	0.382		
12			76.66	24.810					0.89577	89.577
	126.8	38.66			6.459×10^{-2}	1.0346	3.92	0.392		
13			77.59	25.326					0.89969	89.969
	101.8	31.03			6.467×10^{-2}	1.0359	3.15	0.315		
14			78.92	26.069					0.90284	90.284
	106.9	32.58			6.474×10^{-2}	1.0371	3.31	0.331		
15		--	79.73	26.519					0.90615	90.615

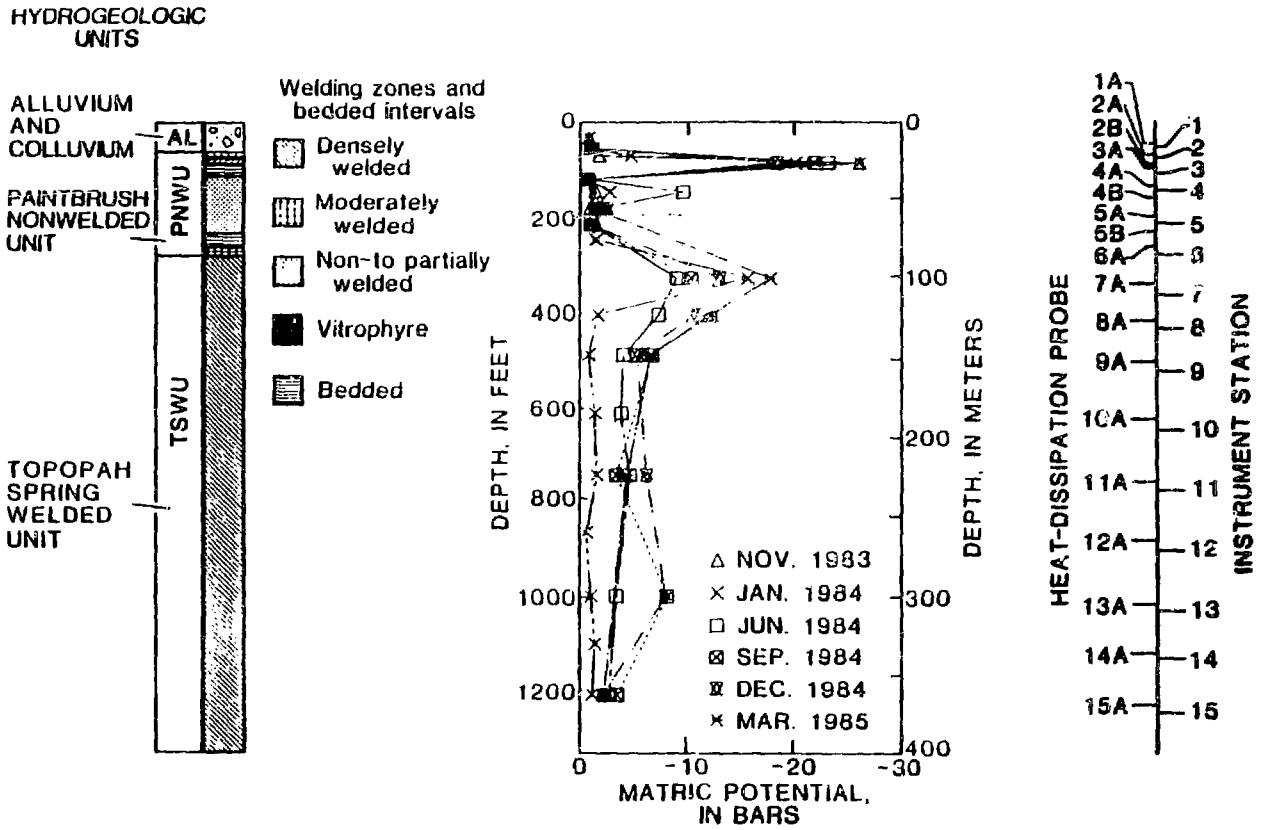

Figure 7.--Matric potential at test borehole USW UZ-1 based on data from heat-dissipation probes.

much shorter than the silica-flour columns in the welded-tuff intervals. The combined effect of these differences probably resulted in the differences in trends detected between the probes placed in the two rock-type intervals. The HDP adjacent to the alluvium and nonwelded tuff probably have reached equilibrium with the formation. However, the HDP in the welded-tuff interval just recently have begun to indicate the movement of water from the formation into the silica flour; this condition is inferred from reversal of the trend from the deeper HDP-8A, HDP-9A, HDP-11A, HDP-3A, HDP-15A. In conclusion, results of the HDP in the alluvium and nonwelded tuff probably represent the formation conditions. The deeper HDP probably are still in a nonequilibrium condition.

Variation of water potentials with depth, measured using TP in the A-screens, are shown for various times in figure 8. All TP except three showed expected trends of dry-to-wet conditions. These three TP (IS-3A, IS-6A, and IS-15A) fluctuated without any trend. Instrument station 15A was located near the bottom of the borehole; the other two (IS-3A and IS-6A) were in bedded tuff in the upper part of the borehole. The TP in the two intervening stations (IS-4A and IS-5A) indicated trends similar to those of the majority of the TP. Individual measurements for the three anomalous instrument stations and for IS-5 are compared in figure 9 (9d through 9g). For IS-3A and IS-6A, early measurements may have represented very dry, rather than very wet, conditions. This situation was possible, because measurements by the TP could represent either very dry or very wet conditions equally well, as a result of measurement and calibration methods (Thamir and McBride, 1985, this proceedings). Inspection of the long-term trends (not shown) indicated that a majority of the TP have stabilized and attained some mean value. Slight deviation from this mean value occurred for some TP. Some deviations of the TP measurements (IS-1A, IS-2A, IS-14A, and IS-15A) consistently indicated gradual drying conditions; at other stations (IS-6A, IS-7A, IS-10A, and IS-13A), deviations of the TP measurements consistently indicated wetting conditions.

Trends for IS-14A and IS-15A (fig. 8) reflected the effects of a 50-ft (15-m) column of cement that was poured to plug the bottom part of the test borehole (Whitfield, 1985, this proceedings). The recent tendency toward drying conditions probably indicated that the formation was drier than the fill material. Instrument stations 1A and 2A also were affected by the water that was used to drill the first 58 ft (17.7 m) of the borehole (Whitfield, 1985, this proceedings). The tendency toward drier conditions probably was indicative of the fact that conditions were drier in the formation than in the fill material. Instrument station IS-3A, which is at a depth of 83 ft (25.3 m), probably was not yet affected by this drilling water (figs. 8 and 9).

Interpretation of the latest matric-potential data measured with HDP and TP is shown in figure 10. This figure was constructed by analyzing individual graphs of matric potential versus time for the duration of the monitoring phase. In some cases, where equilibrium conditions have not been reached, extrapolation of the trend was made to a predicted equilibrium. The left column of this figure is a plot of the fracture traces, as determined from television-camera surveys. Orientation with respect to

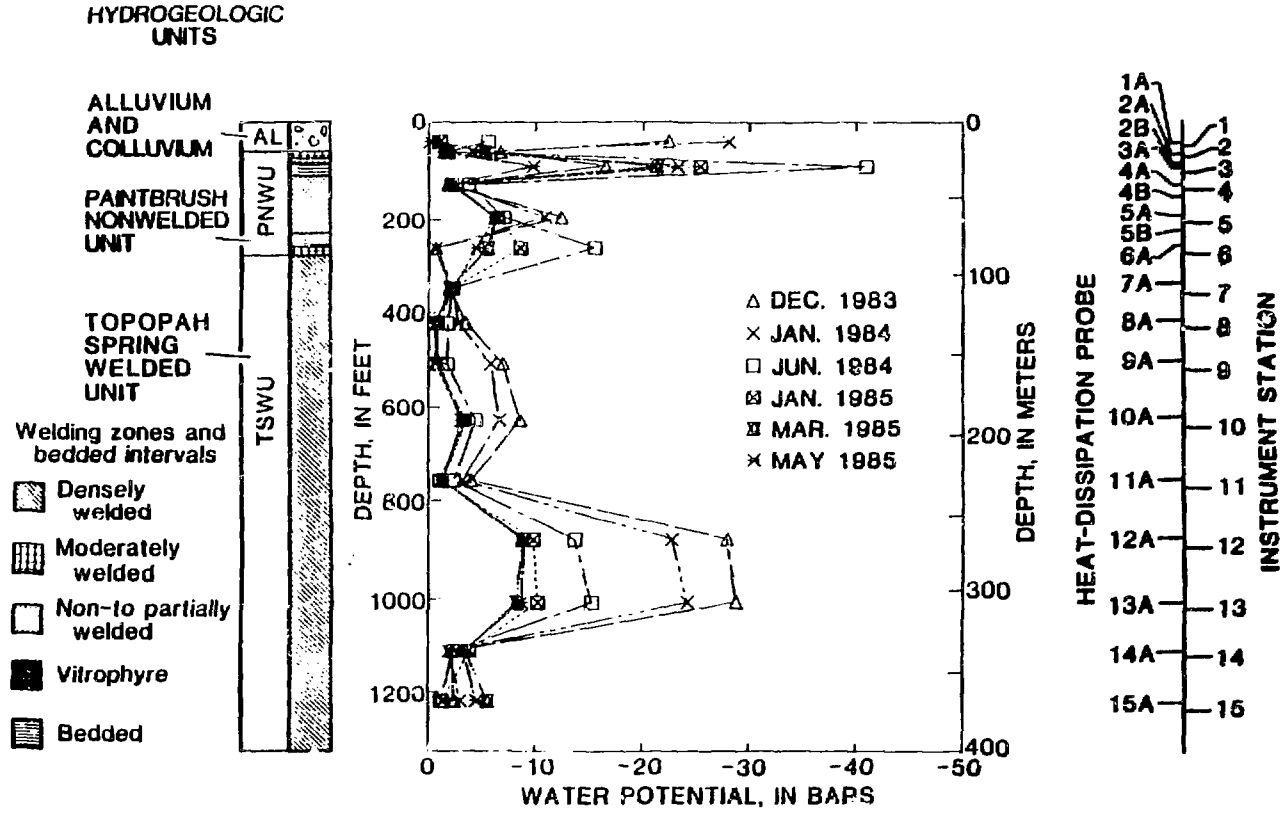

Figure 8.--Water potential at test borehole USW UZ-1 based on data from thermocouple psychrometers.

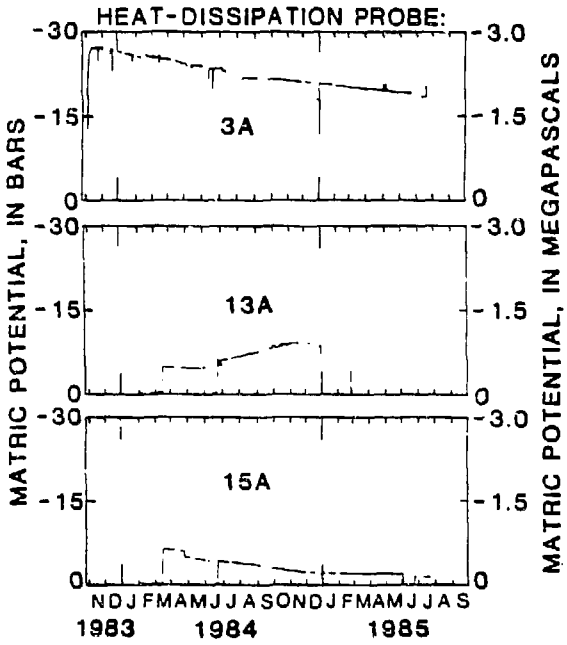

Breaks in data line indicate no data

Figure 9.--Variations of matric potentials with time for selected instrument stations in test borehole USW UZ-1.

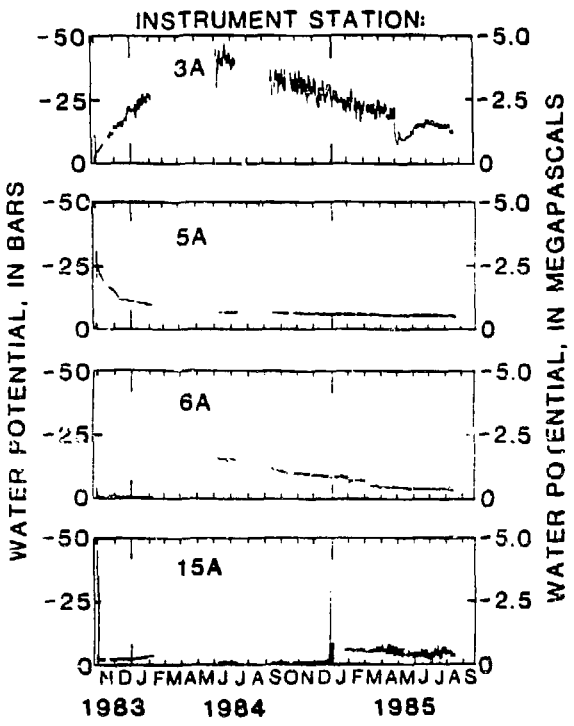

Figure 9.--Variations of water potential with time for selected instrument stations in test borehole USW UZ-1--Continued.

test-borehole axis (nearly vertical), and the trace length of the fractures, are shown with solid lines. As discussed before, the TP measurements probably are more reliable below depths of about 200 ft (61 m). In addition, the TP in A-screens were pumped several times for gas samples; therefore, they were more near equilibrium with the formation than TP in B-screens. The TP installed adjacent to some of the HDP did not perform well, probably because of the ceramic tip that was chosen to minimize contamination from direct contact with silica flour. With these considerations, two regions of steady-state flux could be distinguished within the Topopah Spring welded unit: one between depths of 400 to 800 ft (122 to 244 m), and another below a depth of about 1,000 ft (305 m). No apparent correlation existed between abundance of the fractures and matric-potential distribution. This lack of correlation may have been because matrix flow is dominant in this unit.

Above a depth of about 160 ft (49 m), good agreement existed between TP and HDP measurements. Very dry conditions were indicated for a bedded tuff below alluvium, probably the result of a contrast in hydraulic conductivity of the units. The bedded tuft had greater saturated hydraulic conductivity than did the overlying nonwelded tuff (Montazer and Wilson, 1985, this proceedings); therefore, the bedded tuff could transmit a given flux of water at much smaller matric potential than the nonwelded tuff.

In the depth interval of 400 to 800 ft (122 to 244 m), where a relatively constant matric potential existed within the Topopah Spring welded unit, a flux of water was estimated. The constant matric potential may indicate that a unit hydraulic gradient existed in this interval; if so, the downward flux of water would be equivalent to the effective hydraulic conductivity (Weeks and Wilson, 1984). The average relative permeability of the matrix at ambient matric potential ranged between 0.1 to 0.5 in this interval (Peters et al., 1984). The saturated matrix hydraulic conductivity of the matrix was about 3.3×10^{-6} ft/d (1×10^{-6} m/d, or about 1 mm/yr) (Montazer and Wilson, 1985, this proceedings). Therefore, flux through this interval was about 4×10^{-3} to 2×10^{-2} in./yr (0.1 to 0.5 mm/yr). Weeks and Wilson (1984) estimated 7.9×10^{-3} in./yr (0.2 mm/yr) of flux using matrix properties of the core.

Air Permeability

Weeks (1978) developed a method for determining the vertical permeability of materials to air in the unsaturated zone by monitoring soil-gas pressure fluctuations at depth that were the result of barometric fluctuations at land surface. For this method, the material separating each pair of adjacent screens was assumed to constitute a separate layer with uniform pneumatic properties.

The total pneumatic potentials measured in test borehole USW UZ-1 were suitable for analysis by Weeks' (1978) method, with certain modifications. One modification involved the boundary condition at the base of the system. Surface-induced barometric fluctuations were nearly damped at a depth of 340 ft (104 m), so that no impermeable boundary could be included in the simulation. Consequently, the data were analyzed, beginning with the top two layers, by setting pneumatic potentials at the

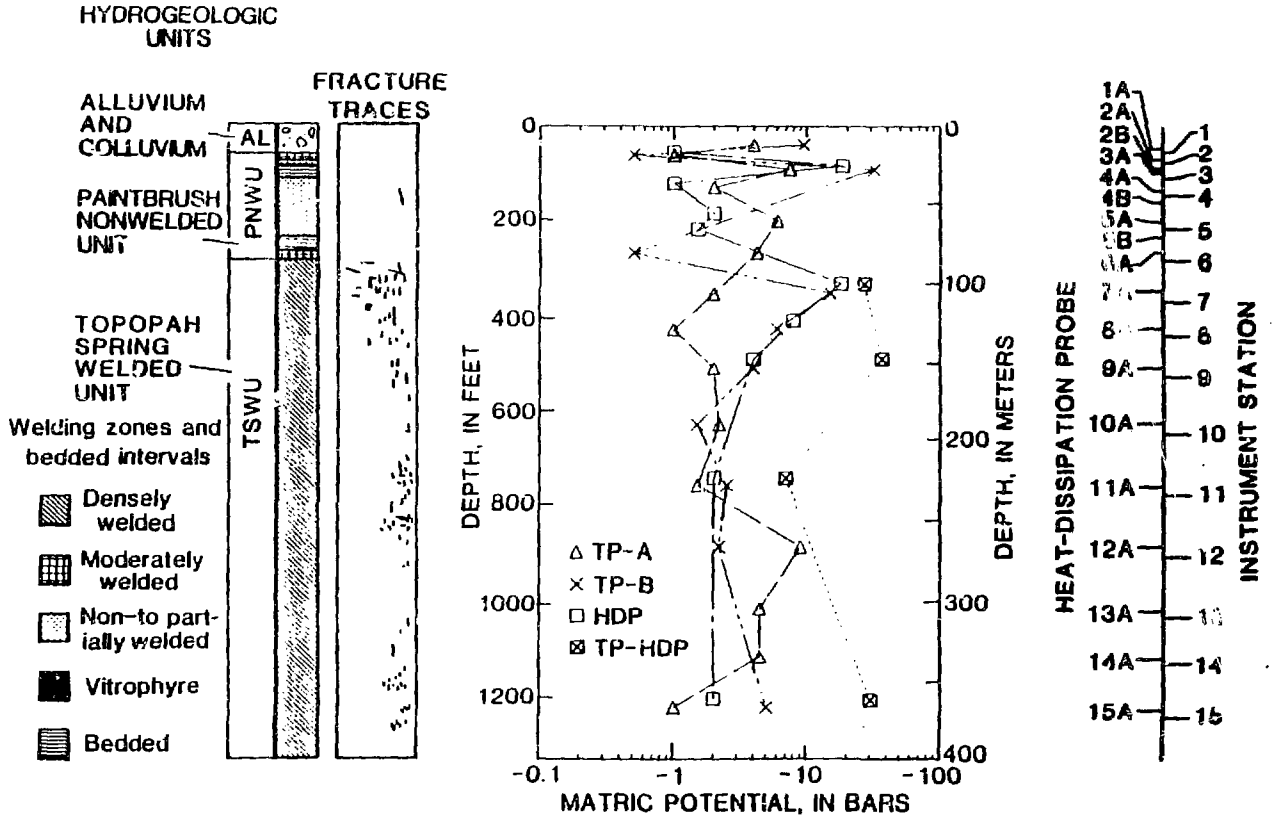

Figure 10.--Distribution of matric potential and fracture traces with depth in test borehole USW UZ-1. The left column shows fracture traces (solid lines) recorded by a television camera. The fracture traces are spread horizontally for clarity only, and do not indicate the position of the fracture with respect to the borehole axis.

base of the second layer and at land surface as boundary conditions. Air-filled porosities were specified for each layer, based on laboratory and neutron-log results. Trial values for the air permeabilities of each layer were used in an initial simulation of the equation for one-dimensional flow of slightly compressible fluids (valid because of the small changes in barometric pressure about the mean) in an attempt to match the pneumatic potential measured in the top screen. Air permeabilities for both layers were varied, using an automatic-search procedure, until the sum of square of deviations between simulated and measured pneumatic potentials changed by no more than a specified value. When this match was obtained, the air permeabilities giving the best fit were fixed for the top two layers.

An additional layer (between IS-2 and IS-3) then was added to the simulation model, with boundary conditions set as pneumatic potentials measured at land surface and at IS-3. Permeability to air of layer 3 then was systematically varied (air-filled porosity being fixed) by the search procedure to obtain a match between measured and simulated potential for IS-2. This procedure was repeated until air permeability for each layer was determined.

Pneumatic potentials measured in test borehole USW UZ-1 were poorly matched by Weeks' (1978) simulation procedure; they appeared to be affected by the slow dissipation of pneumatic potential from fractures or open-flow pathways into a less permeable matrix--a dual-porosity effect. Consequently, the simulation model was modified to incorporate dual porosity, based on the assumptions of Warren and Root (1963) that the pressure change during gas movement from the fracture to the matrix occurs only at the fracture face, but that significant storage occurs within the matrix. The best-fit simulation produced using this model is shown by the symbols in figure 6. The fit to the measured data (lines) is almost exact. The number of layers with dual porosity needed to obtain a good fit was kept to a minimum. Dual porosity was required in the interval from 266 to 340 ft (81 to 104 m), which included densely welded tuff, and in the intervals from 42 to 93 ft (13 to 28 m), 93 to 131 ft (28 to 40 m), and 131 to 201 ft (40 to 61 m), which included nonwelded to partly welded tuff. These data indicate either that the nonwelded to partly welded tuff in these zones was fractured, or that this unit contained preferred flow pathways because of their depositional environment. A comparison between the equivalent hydraulic conductivity estimated at the site of test borehole USW UZ-1 and those estimated at the site of test borehole UE-25a#4 is presented in figure 11. Values of equivalent hydraulic conductivity were derived from values of air permeability using viscosity and density of water at standard conditions.

A piezometer nest was completed in test borehole UE-25a#4, located about 1 mi (1.6 km) southeast of test borehole USW UZ-1. Pneumatic-potential data were collected at that site and analyzed by the method of Weeks (1978). A major difference in the data from the two sites was that there was no indication of the effects of dual porosity at the site of test borehole UE-25a#4. Also, test borehole UE-25a#4 had been drilled with bentonite mud containing a polymer. Thus, some screens were placed in zones that were invaded by drilling mud and determination of barometric fluctuations was not possible; therefore, some thick sequences had to be treated as uniform layers.

The hydraulic conductivity equivalent to the vertical permeability to air is tabulated for both sites in table 2. Permeability data for both sites also are shown relative to the geologic section in figure 11. Hydraulic-conductivity values for the nonwelded tuff at test borehole USW UZ-1 are much larger than those at test borehole UE-25a#4, possibly because of fracturing at the site of test borehole USW UZ-1, particularly because the nonwelded layer, not requiring dual porosity, has relatively small permeability. Simulation results for the welded tuff at the site of test borehole UE-25a#4 indicated that the welded units were much more permeable at this site than at the site of test borehole USW UZ-1.

One problem with the simulation approach used to determine air permeability was that the curve fitting is not sensitive to the absolute values for air permeability for each layer. Permeability ratios, in contrast, are well determined. Thus, all values for a given site may be somewhat larger or smaller by about the same factor.

Thermal Gradient

Variations of temperature with depth are shown in figure 12. For depths between 200 and 1,000 ft (61 and 305 m), temperature measurements after June 1984 were made with TP data loggers. As discussed by Thamir and McBride (1985, this proceedings), this data logger does not measure temperature accurately and these data are not shown in figure 12.

The temperature profiles between depths of about 300 ft to about 1,000 ft (91 to 305 m) generally are convex upward. This curvature can be explained either by variations in thermal conductivity of the geologic units or by an upward flow of vapor-saturated air through the fracture network of the Topopah Spring welded unit. Comparison of these profiles with the frequency of fracture traces (fig. 12) indicates a correlation between frequency of fracture traces and convexity of the profile. The two zones where fractures are most frequent occur at the depth intervals from 300 to 500 ft (92 to 152 m) and from 700 to 900 ft (213 to 274 m). The shallower zone has higher fracture frequency than the deeper zone. Accordingly, the temperature profile of the shallower interval is more convex than the temperature profile of the deeper interval. The temperature measurements made in June 1984, using a special thermister probe in fiberglass tubing (John Sass, U.S. Geological Survey, written commun., 1985), also are shown in figure 12. All temperatures measured with the probe are consistently about 0.5 °C lower than the temperature measurements made by the emplaced thermocouples, for reasons unknown at this time. Nevertheless, both of the convex profiles were reproduced by the second set of measurements; therefore, they probably represent in situ conditions.

Thermal conductivity of this unit was assumed to be uniform throughout its thickness, and a vapor flux was calculated using the methods described by Bredehoeft and Papadopulos (1965), who provided a solution to the equation describing one-dimensional convective-heat transfer. This equation is not strictly applicable to convective flow of gases, and it ignores vapor diffusion. However, for practical purposes, the solution of this equation can be used to approximate one-dimensional natural convection

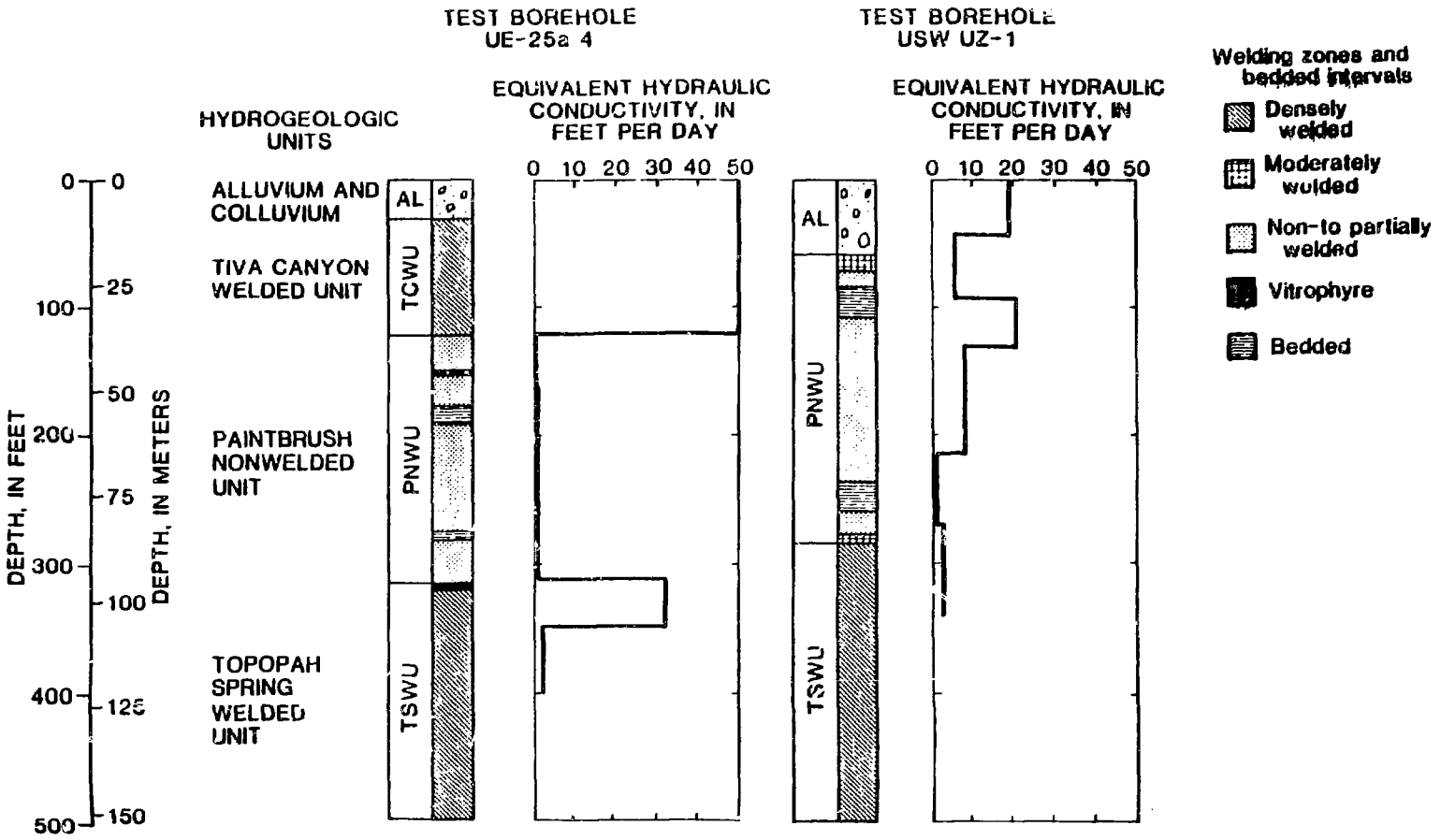

Figure 11.--Permeability of test borehole UE-25a#4 and the upper part of test borehole USW UZ-1 estimated from barometric fluctuations. Lithology after Spengler and Rosenbaum (1980) and R. W. Spengler (U.S. Geological Survey, written commun., 1984).

Table 2.--Results of air-permeability calculations from barometric fluctuations

Depth		Hydraulic conductivity (equivalent)		Air-filled matrix porosity (assumed)	Air-filled fracture porosity
ft	m	ft/d	m/d		
		Test borehole USW UZ-1			
0-42	0-12.8	20	6	0.2	0
42-93	12.8-28.3	7	2	.1	.10
93-131	28.3-39.9	20	6	.22	.03
131-201	39.9-61.3	8	3	.23	.02
201-266	61.3-81.1	.6	.2	.25	0
266-340	81.1-103.6	2	.7	.13	.02
		Test borehole UE-25a#4			
0-124	0-37.8	50	15	0.15	Not considered
124-150	37.8-45.7	.06	.02	.04	Do.
150-313	45.7-95.4	.1	.04	.29	Do.
313-351	95.4-10.0	30	10	.02	Do.
251-399	107.0-121.6	2	.6	.04	Do.

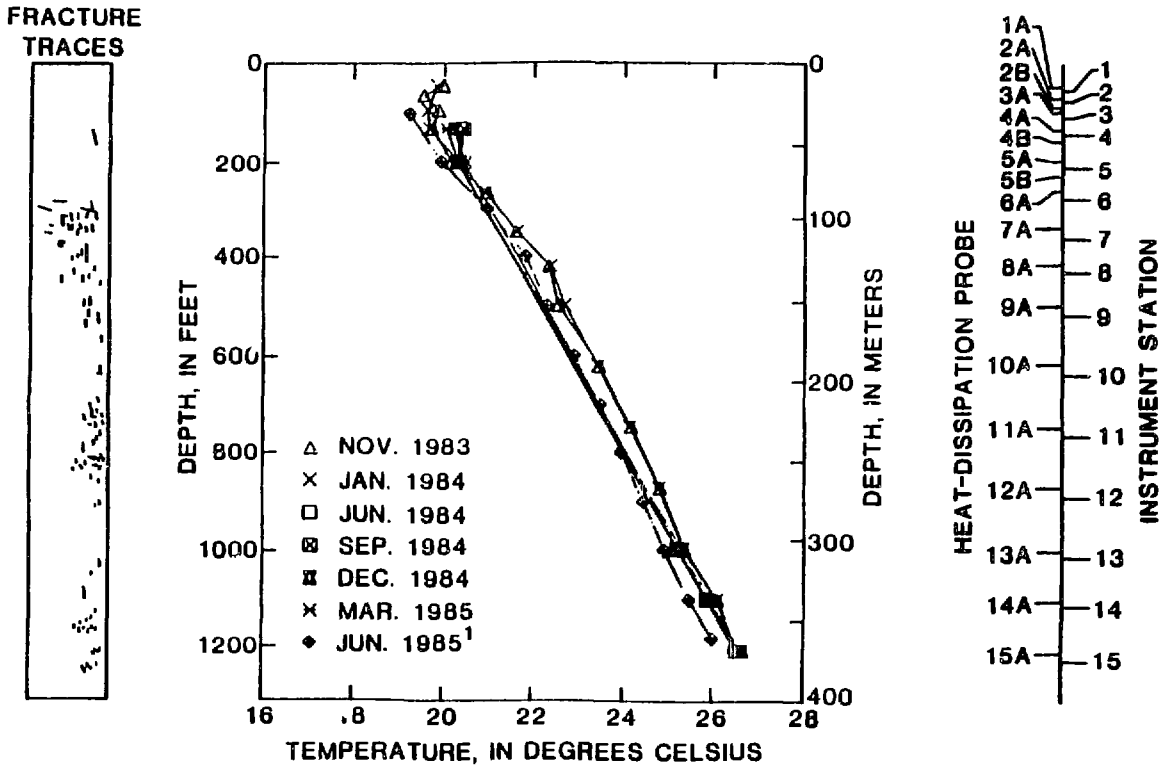

Figure 12.--Temperature profiles and distribution of fracture traces at test borehole USW UZ-1. Data for June 1985 from John Sass (U.S. Geological Survey, written commun., 1985).

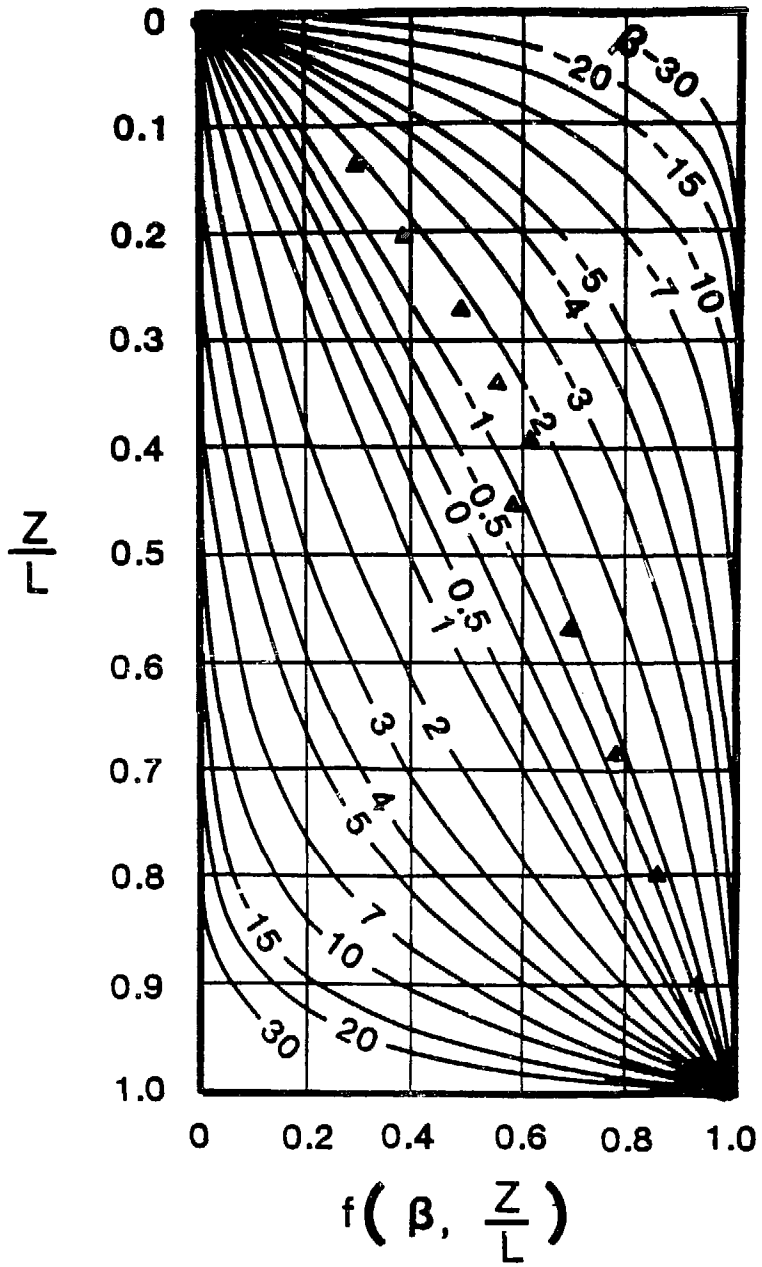

Figure 13.--Type curves of function f(β.z/L) (after Bredehoeft and Papadopulos, 1965) and data from test borehole USW UZ-1 (solid triangles). z is depth; L is thickness of the section considered (1,076 ft, or 328 m, in this case); $\beta = C_o \rho_o v_z L/k$; C_o = specific heat of fluid (0.83 cal/g K for vapor-saturated air); ρ_o is vapor-saturated air density; v_z is air flux; and k is thermal conductivity of the medium (0.0011 cal/cm-s).

of the air, where small temperature and pressure gradients exist. Sorey (1971), using data from Kunii and Smith (1961), demonstrated that this equation can approximate convection of helium. The solution to the equation is provided by Bredehoeft and Papadopulos (1965) in the form of type curves. The type curve closely matching the data from the present study is shown in figure 13, with the parameters used for calculation of the vapor-saturated air flux. The air flux calculated ranges from 49 to 98 in./yr (1,250 to 2,500 mm/yr) upward, depending on the type curve used; β is between 1 and 2. The quantity of water in the form of vapor can be calculated by multiplying these fluxes by the moisture content of the air at saturation, which is approximately 1.24×10^{-3} lb/ft^3 (2×10^{-5} g/cm^3) of dry air at 72°F (22°C). Therefore, the quantity of water that can move upward in the unsaturated zone by these air fluxes is from 1×10^{-3} to 2×10^{-3} in./yr (0.025 to 0.05 mm/yr).

Summary and Conclusions

Fifteen depth intervals were selected in a 17.5-in.- (44.5-cm-) diameter test borehole (borehole USW UZ-1), which was drilled in tuff with a reverse-air vacuum-drilling technique, for emplacement of TP, pressure transducers, and piezometers. An additional 18 depth intervals were selected for emplacement of HDP in silica-flour columns. The TP and pressure transducers were housed in well screens and were embedded in coarse sand. After more than 2 years of monitoring, a majority of the instruments were still functioning and producing reasonable results. Heat-dissipation probes that were placed adjacent to nonwelded tuff and alluvium attained equilibrium faster than those that were placed adjacent to welded tuff. Thermocouple psychrometers produced more reliable data for welded tuff than for nonwelded tuff and alluvium. The results indicated that matric potentials ranged from -0.5 to -25 bars (-0.05 to -2.5 megapascals) in nonwelded tuff and alluvium, and ranged from -2 to -10 bars (-0.2 to -1.0 megapascals) in welded tuff. No apparent correlation existed between matric-potential distribution and frequency of fracture traces observed in the borehole in the welded tuff. Therefore, water flow probably occurred mainly in the matrix of the welded tuff. With this assumption, the water flux through the welded tuff was estimated to be between 4×10^{-3} to 2×10^{-2} in./yr (0.1 to 0.5 mm/yr).

Values of air permeability were estimated from measurements of barometric fluctuations in the test borehole that were detectable to a depth of about 300 ft (91 m). Values of equivalent hydraulic conductivity, calculated from these values of air permeability, ranged from 0.6 to 20 ft/d (0.2 to 6.1 m/d) for nonwelded tuff and alluvium. A single value of 2 ft/d (0.6 m/d) was calculated for the air permeability of the welded tuff. The large air permeability of the nonwelded tuff could be attributed to existence of fractures or other depositional pathways in this unit. However, comparison with data from a nearby test borehole shows that this condition was not pervasive within this unit.

Long-term temperature measurements within this borehole indicated that the geothermal gradient was slightly convex upward within the welded unit. Deviation from the straight line correlated with frequency of fracture traces observed in the borehole. Assuming a uniform thermal conductivity, calculated air fluxes range from -49 to -98 in./yr (-1,250 to -2,500 mm/yr). The quantity of water that could be transported upward by this flux in vapor form was estimated to be from -1×10^{-3} to 2×10^{-3} in./yr (-0.025 to -0.05 mm/yr). This air flux probably occurred through the fractures of the welded tuff.

References

Bredehoeft, J.D. and I.S. Papadopulos. 1965. Rates of vertical groundwater movement estimated from the Earth's thermal profile. Water Resources Research, v. 1, no. 2, pp. 325-328.

Campbell, G.S. 1977. An introduction to environmental biophysics. Springer-Verlag, Inc. New York, NY, 159 pp.

Evans, D.D. 1983. Unsaturated flow and transport through fractured rock--related to high-level waste repositories. Nuclear Regulatory Commission Report NUREG/CR-3206. 231 pp.

Kunii, Daizo and J.M. Smith. 1961. Heat transfer characteristics of porous rocks: II. Thermal conductivities of unconsolidated particles with flowing fluids. American Institute of Chemical Engineers Journal, v. 7, no. 1, pp. 29-34.

Montazer, Parviz. 1982. Permeability of unsaturated fractured metamorphic rocks near an underground opening. Golden, Colorado School of Mines, unpublished Ph.D. Thesis. 617 pp.

Montazer, Parviz and W.E. Wilson. 1984. Conceptual hydrologic model of flow in the unsaturated zone, Yucca Mountain, Nevada. U.S. Geological Survey Water-Resources Investigations Report 84-4345. 55 pp.

Montazer, Parviz and W.E. Wilson. 1985. Hydrogeology of the unsaturated zone, Yucca Mountain, Nevada. in Proceedings, National Water Well Association Conference on Characterization and Monitoring of the Vadose (Unsaturated) Zone, Denver, Colorado, November 19-21, 1985.

Morrison, R.D. 1983. Ground-water monitoring technology--procedures, equipment and applications. Timco Manufacturing, Inc. Prairie DuSac, WI. 111 pp.

Palaz, Ibrahim. 1985. Application of geophysical logs to estimate moisture-content profiles in unsaturated tuff, Yucca Mountain, Nevada. in Proceedings, National Water Well Association Conference on Characterization and Monitoring of the Vadose (Unsaturated) Zone, Denver, Colorado, November 19-21, 1985.

Peters, R.R., E.A. Klavetter, J.J. Hall, S.C. Blair, P.R. Heller and G.W. Gee. 1984. Fracture and matrix hydrologic characteristics of tuffaceous materials from Yucca Mountain, Nye County, Nevada. Sandia Report SAND 84-1471. 63 pp.

Remson, Irwin and J.R. Randolph. 1962. Review of some elements of soil-moisture theory--fluid movement in earth material. U.S. Geological Survey Professional Paper 411-D. 38 pp.

Sorey, M.L. 1971. Measurement of vertical ground-water velocity from temperature profiles in wells. Water Resources Research, v. 7, no. 4, pp. 963-970.

Spengler, R.W. and J.G. Rosenbaum. 1980. Preliminary interpretation of geologic results obtained from boreholes UE25a-4, -5, -6, and -7, Yucca Mountain, Nevada Test Site. U.S. Geological Survey Open-File Report 80-929. 33 pp.

Stallman, R.W. 1964. Multiphase fluids in porous media--A review of theories pertinent to hydrologic studies. U.S. Geological Survey Professional Paper 411-E. 51 pp.

Thamir, Falah and C.M. McBride. 1985. Measurements of matric and water potentials in unsaturated tuff at Yucca Mountain, Nevada. in Proceedings, National Water Well Association Conference on Characterization and Monitoring of the Vadose (Unsaturated) Zone, Denver, Colorado, November 19-21, 1985.

Warren, J.E. and P.J. Root. 1963. The behaviour of naturally fractured reservoirs. Society of Petroleum Engineer's Journal, v. 3, no. 3, pp. 245-255.

Weeks, E.P. 1978. Field determination of vertical permeability to air in the unsaturated zone. U.S. Geological Survey Professional Paper 1051. 41 pp.

Weeks, E.P. and W.E. Wilson. 1984. Preliminary evaluation of hydrologic properties of cores of unsaturated tuff, test well USW H-1, Yucca Mountain, Nevada. U.S. Geological Survey Water-Resources Investigations Report 84-4193. 30 pp.

Whitfield, M.S. 1985. Vacuum drilling of unsaturated tuff at a potential radioactive waste repository, Yucca Mountain, Nevada. in Proceedings, National Water Well Association Conference on Characterization and Monitoring of the Vadose (Unsaturated) Zone, Denver, Colorado, November 19-21, 1985.

Yang, In C., H.H. Haas, E.P. Weeks and D.C. Thorstenson. 1985. Analysis of gaseous-phase stable and radioactive isotopes in the unsaturated zone, Yucca Mountain, Nevada. in Proceedings, National Water Well Association Conference on Characterization and Monitoring of the Vadose (Unsaturated) Zone, Denver, Colorado, November 19-21, 1985.

Biographical Sketch

Parviz Montazer received his Bachelor of Science from Pahlavi University, Shiraz, Iran, in 1972, and his Master of Science and Doctor of Philosophy degree from Colorado School of Mines, Golden, Colorado, in geological engineering in 1978 and 1982, respectively. He has been employed by the Water Resources Division of the U.S. Geological Survey in Denver, Colorado since 1983. His research interests include flow through fractured rocks and hydrology of deep unsaturated zones. He is currently the Project Chief for Unsaturated-Zone Hydrologic Studies of Yucca Mountain, Nevada Test Site. His address is: U.S. Geological Survey, Box 25046, MS 416, Denver Federal Center, Denver, Colorado 80225.

Edwin Weeks received his Bachelor of Science in geological engineering from Colorado School of Mines, Golden, Colorado in 1958. He has worked in various aspects of ground-water research at the Water Resources Division of the U.S. Geological Survey from 1958 to present. Since 1958, he has served as the chief of various projects involving studies of the impacts of irrigation on ground-water systems, development of air-permeability techniques to characterize unsaturated zones, investigation of artificial

recharge methods, studies of anisothermal vapor transport and gaseous diffusion in the unsaturated zone, and measurement of evapotranspiration. He has also taught courses at the U.S. Geological Survey Training Center in various ground-water related subjects. He is currently Chief of the Unsaturated Zone Field Studies in Denver, Colorado. His address is: U.S. Geological Survey, Box 25046, MS 413, Denver Federal Center, Denver, Colorado 80225.

Falah Thamir received his Bachelor of Science from the University of Baghdad, Iraq, in 1977, and his Master of Science from Colorado School of Mines in Golden, Colorado in 1984 in mining engineering. He is currently employed by Goodson and Associates in Denver as a contract engineer for the U.S. Geological Survey, Nuclear Hydrology Program. His address is: U.S. Geological Survey, Box 25046, MS 416, Denver Federal Center, Denver, Colorado 80225.

Stephanie N. Yard has been employed by Goodson and Associates, Inc., as a contract employee for the U.S. Geological Survey in Denver, Colorado, since 1984. She is a student at the University of Colorado at Denver, pursuing a Bachelor of Science degree in civil engineering. Her address is: U.S. Geological Survey, Box 25046, MS 416, Denver Federal Center, Denver, Colorado 80225.

(Biographical information for P.B. Hofrichter was unavailable at press time.)